RSC Advances

PAPER

View Article Online
View Journal | View Issue

Cite this: *RSC Adv.*, 2025, **15**, 2175

Engineering $0.8BiFeO_3–0.2BaTiO_3$ multiferroics with improved dielectric and magnetic properties *via* samarium doping

Houda Krir,[a] F. Gadhoumi,*[a] N. Abdelmoula,[a] M. Tabellout,[b] H. Khemakhem[a] and N. Randrianantoandro[b]

Received 13th November 2024
Accepted 17th December 2024

DOI: 10.1039/d4ra08068h

rsc.li/rsc-advances

Samarium (Sm) modification is emerging as a powerful strategy to manipulate the electrical response of $0.8BiFeO_3–0.2BaTiO_3$ (BFBT) multiferroic ceramics. In this work, Sm-doped BFBT (BFBT05Sm and BFBT01Sm) are successfully synthesized *via* the solid–state reaction technique. X-ray diffraction (XRD) analysis coupled with Rietveld refinement confirms the formation of a pure perovskite structure with rhombohedral symmetry (*R3c* space group) for all compositions, indicating the effective integration of Sm into the BFBT lattice. In particular, scanning electron microscopy (SEM) reveals a remarkable increase in grain size upon Sm doping, reaching 1.098 μm in BFBT01Sm compared to 0.192 μm in the BFBT sample. Further evidence for the *R3c* space group comes from Raman spectroscopy, which reveals identical vibrational modes in all samples. Most importantly, the Sm substitution significantly reduces the dielectric loss compared to BFBT. A comprehensive analysis of the Mössbauer spectral parameters reveals the influence of Sm doping on the magnetic interactions.

1. Introduction

Recently, multiferroic materials that exhibit more than one ferroic order-such as ferroelectric, antiferromagnetic, or ferroelastic materials have attracted considerable attention. Their unique combination of ferroelectric and magnetic properties makes them promising candidates for advanced electronic applications, including data storage, actuators, sensors, and ultra-high-speed telecommunications.[1–3]

Bismuth ferrite $BiFeO_3$ (BFO) is the most attractive multiferroic material with both ferroelectric and magnetic properties in the same perovskite structure at ambient temperature. It exhibits a rhombohedral distorted ABO_3-type perovskite structure (*R3c*). BFO exhibits ferroelectricity at high Curie temperatures ($T_C \sim 829.85$ °C) and G-type antiferromagnetic properties ($T_N \sim 369.85$ °C) [4,5]. The origin of the antiferromagnetic order arises from the cycloidal spin structure with a long period of 62 nm, resulting in weak macroscopic magnetization and a weak magnetoelectric effect. Researchers have explored various strategies to overcome these limitations and improve the performance of BFO. These approaches include improving preparation methods (such as the fast liquid phase method,[4] microwave method, sol–gel, *etc.*), substituting different ions at A or B sites,[5,6] and creating solid solutions with other ABO_3-type perovskite structures (such as $BaTiO_3$ (BTO) and $SrTiO_3$). Solid solutions with $BaTiO_3$ have successfully suppressed impurity formation and improved electrical insulation.[7]

We have conducted extensive research in this area, driven by the promising technological potential of $BiFeO_3–BaTiO_3$ (BFBT) ceramics and their multiferroic properties. In our previous study, we investigated the effects of the rare earth Europium doping on these ceramics and achieved significant improvements.[8] In addition, Samarium belongs to the rare earth which may also has an important application in solid state devices by improving magnetic and dielectric properties. Samarium has a smaller ionic radius (0.96 Å) than bismuth (1.08 Å), which can introduce lattice strain when it partially replaces Bi^{3+} in the crystal structure. This strain modifies the material's structure, promoting stronger ferroelectric polarization and enhancing magnetic interactions. Additionally, many works have been done about Sm substituted $BiFeO_3$ to improve multiferroic properties.[9,10] K. S. Nalwa *et al.* [11] reported that Sm doping eliminated impurity phases leading to the formation of perovskite Sm-doped $BiFeO_3$ phase. Therefore, Sm substitution optimizes the dielectric and magnetic performance of the BFO–BT matrix while ensuring the structural stability essential for practical applications such as Photocatalysis[12] and photovoltaics harvesting.[13]

Based on these results, the present study investigates the effect of samarium doping on BFBT ceramics. In order to

[a]*Laboratory of Multifunctional Materials and Applications (LaMMA), (LR16ES18), Faculty of Sciences of Sfax, University of Sfax, B. P. 1171, Sfax, 3000, Tunisia*
[b]*IMMM, Institut des Molécules et Matériaux du Mans Bd Charles Nicolle, 72000 Le Mans, France*

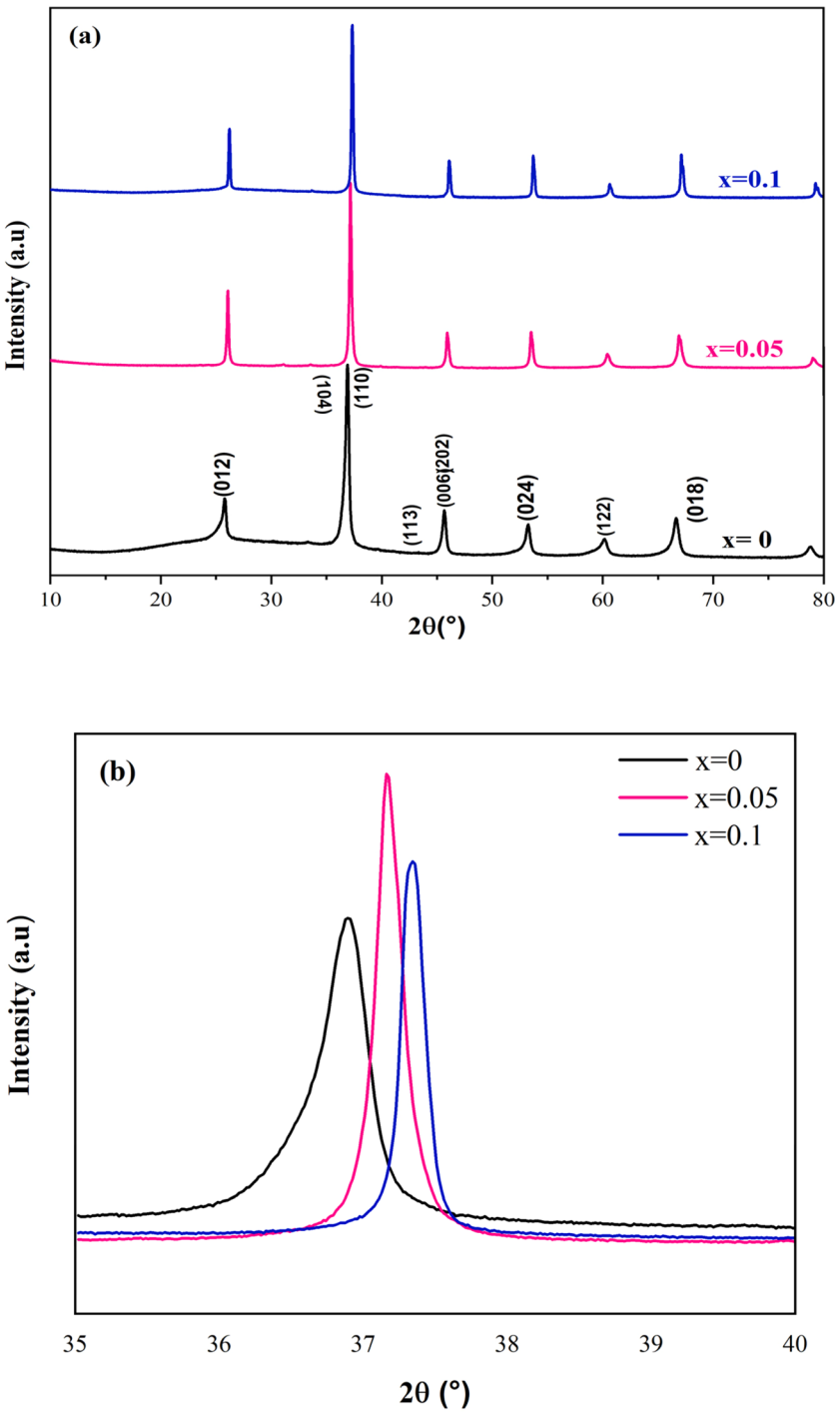

Fig. 1 XRD patterns (a) and magnified view of (110) diffraction peak (b) of BFBT, BFOBT05Sm, and BFBT01Sm compounds.

optimize their performance, Sm-doped 0.8BFO–0.2BT ceramics with different Sm_2O_3 contents (x = 0, 0.05, and 0.1) were synthesized. A comprehensive analysis of their structural, electrical, and magnetic properties is presented to elucidate the influence of Sm doping on material performance and to pave the way for further optimization of BFBT ceramics for advanced technological applications.

2. Experimental details

2.1. Sample preparation

We have synthesized 0.8BFO–0.2BT ceramics doped with Sm_2O_3 (x = 0, 0.05, and 0.1) using the conventional high-temperature solid state reaction technique. Stoichiometric amounts of Bi_2O_3 (99.0%, Aldrich), $BaCO_3$ (99.9%, Aldrich), Fe_2O_3 (99.0%, Aldrich), TiO_2 (99.9%, Aldrich), and Sm_2O_3 (99.99%, Aldrich)

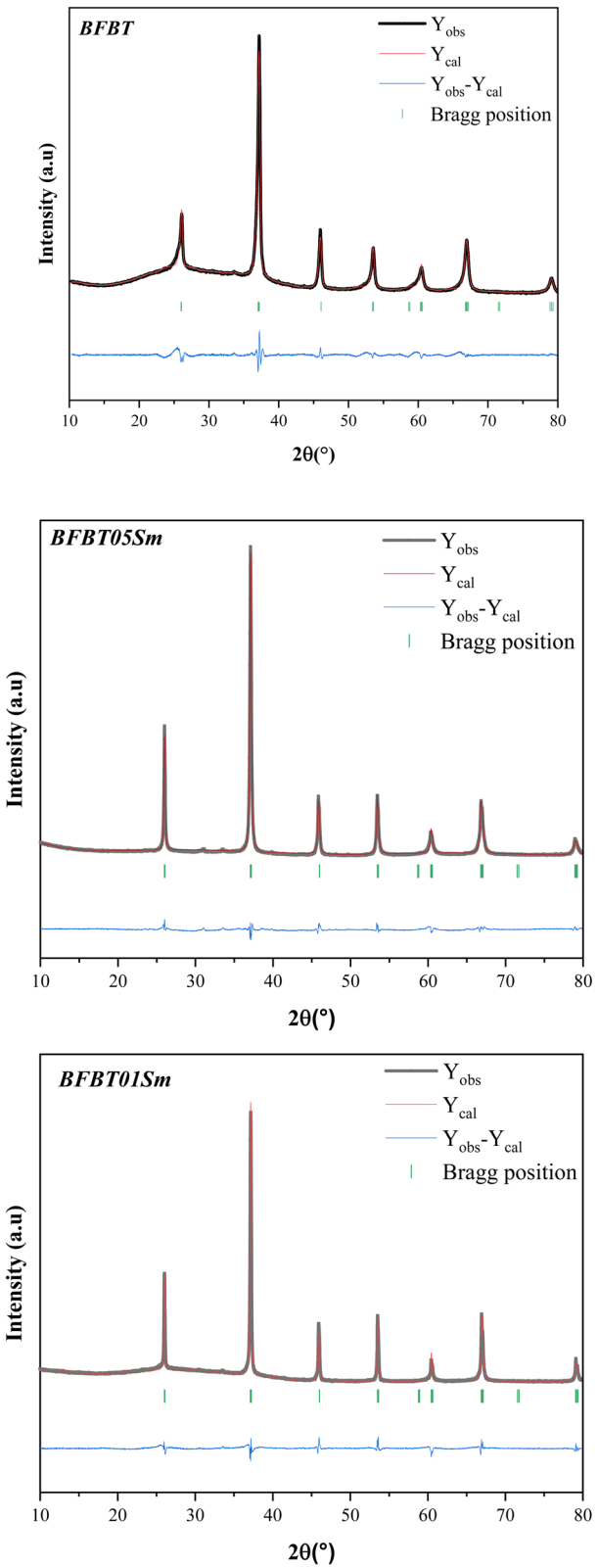

Fig. 2 X-ray diffraction patterns of BFBT, BFBT05Sm, and BFBT01 Sm at room temperature.

were mixed in an agate mortar for 2 h, and then calcined at 600 °C, 700 °C, and 800 °C for 2 h. The powders were weighed after calcination. After calcination, the powders were mixed for 3 hours and compacted under 100 MPa pressure into pellets 8 mm in diameter and approximately 1 mm thick. The resulting pellets were annealed at 1000 °C for 2 hours.

2.2. Measurement tools

The crystal structure of sintered samples was analyzed using a PANalytical X'Pert diffractometer with a cobalt target (λ = 1.7889 Å). Rietveld refinement was conducted using FULLPROF software.

Raman spectra were obtained for all samples using a Horiba Jobin-Yvon (HR 800UV) micro-Raman spectrometer using a 632 nm excitation line from a He–Ne laser. All spectra were collected at room temperature in the 50–800 cm^{-1} range.

Powder morphology was examined using a TESCAN VEGA3 SBH scanning electron microscope (SEM) with a Bruker XFlagh 410 M EDS detector.

The dielectric data were collected for the silver-coated samples in a planar configuration using a Wayne Kerr 6425 component analyzer.

Magnetic measurements were performed using a Quantum Design MPMS-XL-7CA SQUID magnetometer. Mössbauer spectrometry was carried out at RT in standard transmission geometry using a Co source diffused in a rhodium matrix. The data obtained from Mössbauer spectroscopy were analyzed using MOSFiT software.

3. Results and discussions

3.1. Structural and microstructure analysis

The assessment of phase purity for the $0.8(Bi_{(1-x)}\ Sm_xFeO_3)$–$0.2BaTiO_3$ for x = 0, 0.05, and 0.1 compounds series was carried out using room-temperature powder XRD spectra. As depicted in Fig. 1, the XRD patterns of all BFBT, BFBT05Sm, and BFBT01Sm exhibit the typical perovskite structure, indicating the successful integration of Sm into the BFBT ceramic compound system. The crystal structure of the composition x = 0 has been studied in our previous work.[8] It was found that this sample crystallized in a rhombohedral structure with the space group *R3c*. In other works,[14–16] it is reported that $(1-x)$ $BiFeO_{3-x}$ BT systems display rhombohedral structure. Then, the structure transforms to cubic at 33 mol% of BaTiO3 and again transforms to tetragonal, as the other end of the system is reached, *i.e.* $BaTiO_3$. Therefore, the analysis of the characteristic diffraction peaks reveals that all ceramic samples exhibit a rhombohedral arrangement within the *R3c* space group, devoid of any discernible impurity phases. This observation suggests successful diffusion of Sm into the lattice, resulting in the formation of homogeneous compounds. This finding aligns with prior research, indicating that doping with rare-earth elements can effectively suppress the formation of secondary phases.[17] Moreover, as the Sm content increases, the diffraction peaks of the samples shift towards higher angles. Fig. 1b shows the displacement of the pic at $2\theta \sim 37°$ implying a reduction in lattice spacing and lattice constant with the increasing doping concentration. To determine the refinement parameters of BFBT05Sm and BFBT01Sm, Rietveld analysis

Table 1 Table of refinement parameters

Samples	Lattices parameters (Å) and volume (Å^3)	Atomic positions				Average bond length (Å)	Bond angles (deg)	*R*-Facteurs
			x	*y*	*z*			
BFBT	$a = b = 5.632(0)$	Bi/Ba	0.00	0.000	0.254(6)	Bi–O 2.624(6)	Fe–O–Fe 156.24(0)	$R_P = 2.71$
	$c = 13.750(3)$	Fe/Ti	0.00	0.000	0.000	Fe–O 1.989(2)		$R_{WP} = 3.65$
	$V = 377.723$ (0)	O	0.103(8)	0.283(1)	0.132(8)	Fe–O 2.075(0)		$R_{exp} = 2.76$
								$\chi^2 = 1.75$
BFBT05Sm	$a = b = 5.624(2)$	Bi/Ba/Sm	0.000	0.000	0.259(3)	Bi–O 2.588(1)	Fe–O–Fe 155.20(0)	$R_P = 2.93$
	$c = 13.790(2)$	Fe/Mn	0.000	0.000	0.000	e–O 2.013(0)		$R_{WP} = 3.83$
	$V = 377.760(3)$	O	0.096(4)	0.288(1)	0.102(8)	FFe–O 2.062(1)		$R_{exp} = 2.52$
								$\chi^2 = 1.19$
BFBT01Sm	$a = b = 5.616(4)$	Bi/Ba/Sm	0.000	0.000	0.255	Bi–O 2.446(6)	Fe–O–Fe 131.65(2)	$R_P = 4.16$
	$c = 13.776(5)$	Fe/Mn	0.000	0.000	0.000	Fe–O 2.155(0)		$R_{WP} = 5.44$
	$V = 376.348(0)$	O	0.196(2)	0.298(5)	0.113(9)	Fe–O 1.950(0)		$R_{exp} = 3.45$
								$\chi^2 = 2.48$

was carried out (as shown in Fig. 2). The refinement parameters, encompassing lattice parameters, bond angles, average bond lengths, and R-factors derived from X-ray diffraction data, are presented in Table 1. The results show that the ceramics crystallize in a rhombohedral shape with the space group *R*3*c*, indicating successful refinements. It can be noted a variation in lattice parameters and cell volume. When Bi^{3+} ions (with an ionic radius of 0.117 nm) at the A-site are substituted by Sm^{3+} ions (with an ionic radius of 0.096 nm), the lattice constant tends to decrease compared to the BFBT system.

From Rietveld analysis, we could calculate the average crystallite size (D) and the microstrain (ε) using the following equations:[18]

$$D = \frac{k\lambda}{\beta \cos \theta} \quad (1)$$

$$\varepsilon = \frac{\beta}{4 \tan \theta} \quad (2)$$

where $k = 0.9$ is the shape factor, λ is the X-ray wavelength (λ = 1.7891Å), β is the full width at half-maximum, and θ is the Bragg angle. The calculated values are illustrated in Table 2. The increase in crystallite size with Sm content is observed. This result can be explained by the local distortion that occurred after Sm substitution.[19]

The SEM examination shows that all ceramic samples have densely packed and compact microstructures with minimal to no observable pores. This phenomenon could be attributed to the change in microstructure after Sm doping. Using ImageJ software,[20] the average grain size was estimated for all samples. The analysis revealed a significant increase in grain size from 0.192 μm observed in the BFBT sample to 0.622 μm and 1.098 μm in the BFBT05Sm and BFBT01Sm samples, respectively. This increase is probably due to the addition of Sm; which can cause densification of the material, then the grains are more compact. the microstructure becomes uniform. Also, the grain growth is likely explained by synthesis condition such as temperature sintering. Indeed, when the sintering temperature is higher it promotes grain growth by providing sufficient energy for atoms to migrate across boundaries, thus overcoming energy barriers associated with grain boundary interactions.[21] Moreover Sm doping reduces lattice stress and promotes densification, leading to better grain boundary interactions and refined grain morphology during sintering.[12,22] In summary, moderate levels of Sm doping can ensure high density and enhance grain sizes, thereby potentially improving the electrical properties of BFBT-based ceramics.[1,23] In addition, an energy dispersive X-ray or EDS was used to analyze the

Table 2 Crystallite size and micro-strain values for all samples

Samples	BFBT	BFBT05Sm	BFBT01Sm
Crystallite size (μm)	24.181	63.580	76.044
Micro-strain ($\times 10^{-3}$)	5.470	2.080	1.740

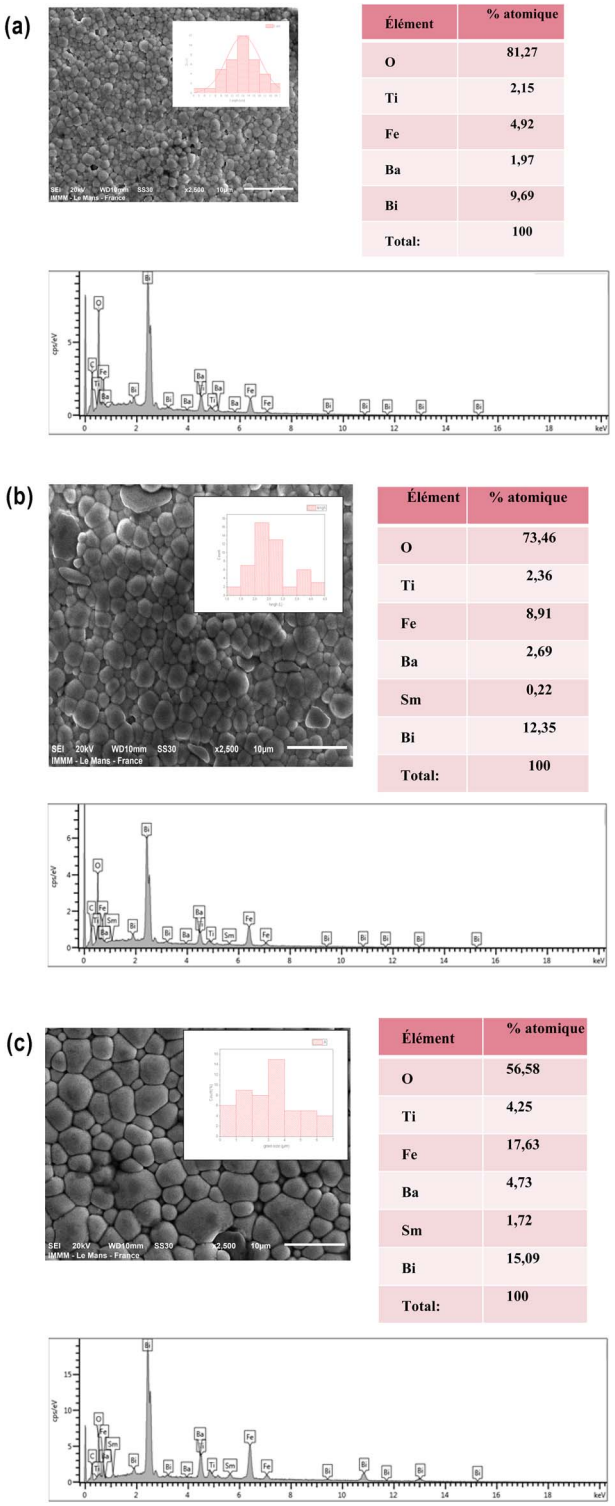

Fig. 3 SEM images, histograms, and EDS analysis for compounds BFBT (a) and BFBT05Sm (b) BFBT01Sm (c).

elements of the ceramics. The presence of distinct peaks for Bi, Ba, Sm, Fe, Ti, and O in the same figure shows that no elements were lost during the reactions and no impurity elements were found (Fig. 3).

3.2. Raman Spectroscopy

Fig. 4 shows the Raman vibrational modes ranging from 100 to 1200 cm^{-1} for the BFBT, BFBT05Sm and BFBT01Sm compounds. According to group theory, the rhombohedral phase contains 13 different Raman active vibrational modes.[24] $BiFeO_3$ has a crystal lattice where Bi^{3+} ions occupy specific sites, usually in an oxygen-coordinated environment. When the Bi^{3+} ion is substituted by a Sm^{3+} ions, several structural changes can occur. To characterize the effect of Sm^{3+} doping on the atomic vibrations, the Raman spectrum of BFBT05Sm and BFBT01Sm ceramics were deconvoluted using a Lorentzian profile. Only 9 peaks could be distinguished. This limitation was mainly due to the overlapping of different modes.[25] In fact, the difference in ionic radius of Bi and Sm can cause a local lattice distortion around the substituted site. As a result, the substitution can affect the coordination of cations and lead to changes in the symmetry of the crystal lattice. Additionally, it can be noted the observation of two distinct peaks in the region 200–400 cm^{-1}. These peaks are probably related to changes in lattice distortion, cation coordination and vibration modes of FeO_6 octahedra.[26]

Moreover, a pronounced pic is observed in the vicinity of 800 cm^{-1} for BFBT05Sm and BFBT01Sm compounds. This observation can be explained by the stretching of FeO_6 octahedra. Therefore, the Raman spectroscopy observations strongly support the crystal structure XRD data.

3.3. Dielectric study

Dielectric analysis is critical in determining the electrical properties of ceramics. Fig. 5 shows the temperature dependent dielectric permittivity (ε_r) and tangent loss (tan δ) of BFBT05Sm and BFBT01Sm ceramics at various frequencies (10 Hz to 100 kHz). The dielectric constant values decrease with increasing frequency. This is due to dipole relaxation, where at lower frequencies the dipoles can keep up with the frequency of the applied field.[27] An anomaly can be observed near 225 °C. This temperature can be attributed to the Néel temperature (T_N), where the magnetic ordering of the BFBT changes.[28] Notably, this anomaly is significantly reduced for BFBT05Sm and BFBT01Sm (shifted to a lower temperature). The presence of another anomaly in the dielectric constant value near the magnetic transition temperature ($T_c \approx 397$ °C) for the 0.8BFO–0.2BT composition indicates a coupling between ferroic orders during the paramagnetic–antiferromagnetic transition.[29] Zhuang Ma's research suggests the presence of another anomaly around 400 °C, which could be the Curie temperature (T_c).[19] However, our equipment limitations prevented us from detecting this anomaly, as it cannot reach temperatures above 400 °C. The relaxor behavior of BFBT ceramics has been attributed to the disordered distribution of Bi^{3+} and Sm^{3+} ions at the A-site, which enhances the random local fields and leads to the formation of polar nanoregions (PNRs). This phenomenon, induced by structural disorder, has also been reported in similar studies, further supporting the connection between disordered ion distribution and the formation of PNRs in relaxor materials.[17,30]

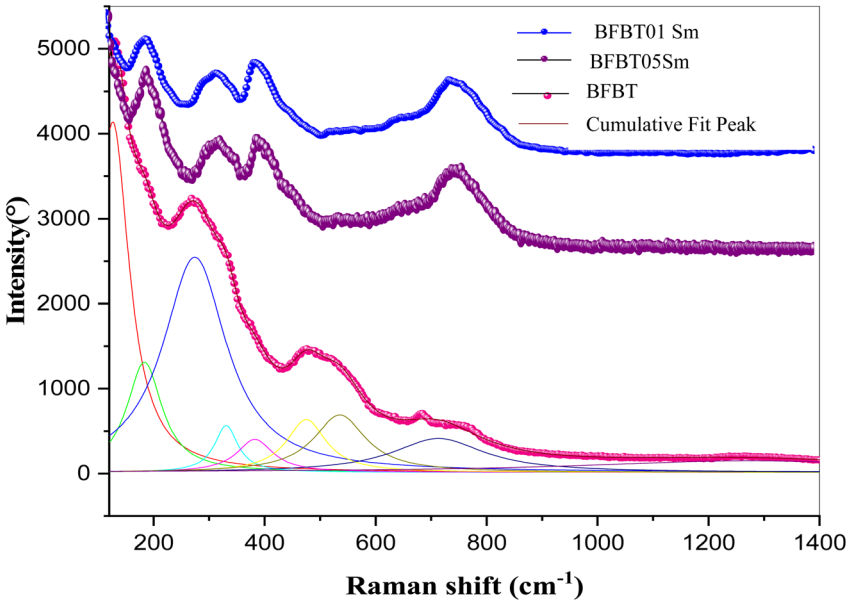

Fig. 4 Raman spectra of BFBT, BFBT05Sm, and BFBT01Sm ceramics at room temperature.

Our analysis of the dielectric loss (tan δ) *versus* temperature, as shown in the inset for each curve in Fig. 5, reveals a clear temperature dependence. At low temperatures, the values remain low, then increase sharply with temperature. Such behavior suggests potential contributions from two phenomena: thermally activated charge carrier scattering and the presence of unidentified defects within the material, such as oxygen vacancies.[31] Correspondingly, a significant decrease in the dielectric loss after the substitution of Sm compared to 0.8BFO–0.2BT. For example, at 10 kHz, the BFBT sample exhibits a tan δ of approximately 0.22, this value progressively decreases to 0.15 for BFBT05Sm and further reduces significantly to around 0.092 for BFBT01Sm. This enhancement in dielectric properties due to Sm content can be explained by the reduction of conductivity in the material. Replacing Bi^{3+} with Sm^{3+} effectively reduces both the volatilization of Bi^{3+} ions and the formation of oxygen vacancies.[32]

3.4. Mössbauer spectroscopic study

To study the hyperfine magnetic properties and oxidation states of iron atoms ^{54}Fe,[33] Mössbauer spectroscopy was utilized to analyze both undoped and doped BFO–BT ceramics. The Mössbauer spectra obtained for these materials at room temperature are depicted in Fig. 6.

The Mössbauer spectra obtained for all samples displayed a combination of a sextet (six-line pattern). The sextet can be attributed to the Zeeman splitting of the iron nuclear energy levels, arising from the presence of a hyperfine magnetic field. This observation indicates the existence of magnetic ordering, potentially a helical or slightly canted antiferromagnetic structure with a Néel temperature (T_N) expected to be above room temperature. A comprehensive analysis of the Mössbauer spectral parameters encompassing the isomer shift (δ), line width at half maximum (Γ), quadrupole splitting QS (Δ), magnetic hyperfine field (B_{hf}), and relative spectral area contributions, is presented in Table 3 for the BFBT, BFBT05Sm, and BFBT01Sm samples. The isomer shift I.S. (δ) numerical value indicates the valence state of iron atoms. For Fe^{2+}, the I. S. ranges from 0.6 to 1.7 mm s^{-1}, while for Fe^{3+}, it falls between 0.05 and 0.5 mm s^{-1}, and for Fe^{4+}, it is between −0.15 and 0.05 mm s^{-1}.[34,35] In this study, the isomer shift (I. S.) values for BFBT, BFBT05Sm, and BFBT01Sm are 0.509, 0.501, and 0.549, respectively, indicating the presence of iron in the Fe^{3+} oxidation state. After the addition of samarium (Sm), the values of the quadrupole splitting (Q. S.) did not show significant change. This observation suggests that samarium integrates harmoniously into the crystal structure without significantly disturbing the lattice parameters. Consequently, the addition of Sm does not induce notable distortion in the crystal structure, thus preserving the intrinsic properties of the material while potentially enhancing other desirable characteristics.[36] Furthermore, the slight decrease in B_{hf} observed in BFBT05Sm and BFBT01Sm, compared to undoped BFO, can be attributed to local distortions around the Fe sites. These distortions likely arise due to the presence of Bi vacancies, which aligns with observations reported in other studies.[35,37] As illustrated in Fig. 6a, the Mössbauer spectrum of BFBT reveals a marked asymmetry characterized by a notable intensity difference between lines (1) and (6), and (2) and (5). This asymmetry is associated with cycloidal modulation.[38,39] In contrast, the spectra of the doped compounds BBFBT05Sm (Fig. 6b) and BFBT01Sm (Fig. 6c) exhibit increased symmetry. These observations suggest that the present doping has the potential to mitigate the modulated spiral spin structure of BFO.[39] A similar trend is observed in other doped BFO compounds, such as Y-doped BFO[40] and Pr-doped BFO.[41]

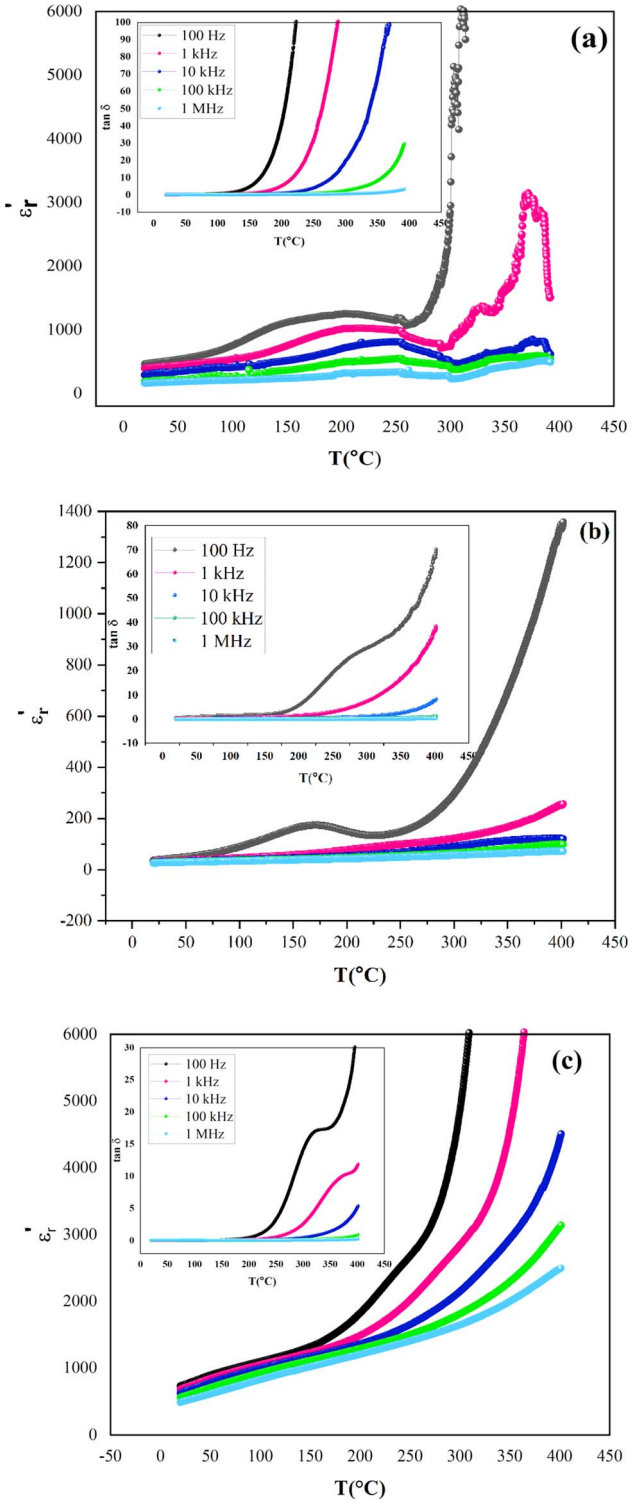

Fig. 5 Variation of ε_r with temperature at different frequencies for BFBT (a), BFBT05Sm (b) and BFBT01Sm (c). The inset shows the corresponding tan δ *versus* T.

4. Conclusion

The successful synthesis of Sm-doped $0.8BiFeO_3$–$0.2BaTiO_3$ (BFBT) ceramics demonstrates the significant influence of samarium modification on the structural, electrical and magnetic properties of the material. The incorporation of Sm not only preserves the perovskite structure with rhombohedral symmetry, but also significantly increases the grain size, as confirmed by SEM analysis. This structural modification is accompanied by a significant reduction in dielectric loss, highlighting the potential of Sm doping to optimize the electrical performance of BFBT ceramics. In addition, Mössbauer spectroscopy reveals the change in magnetic interactions due to Sm substitution, which further contributes to the multiferroic behavior of the material. These results solidify Sm doping as a robust approach for tailoring the properties of BFBT ceramics, paving the way for their potential applications in advanced multifunctional devices.

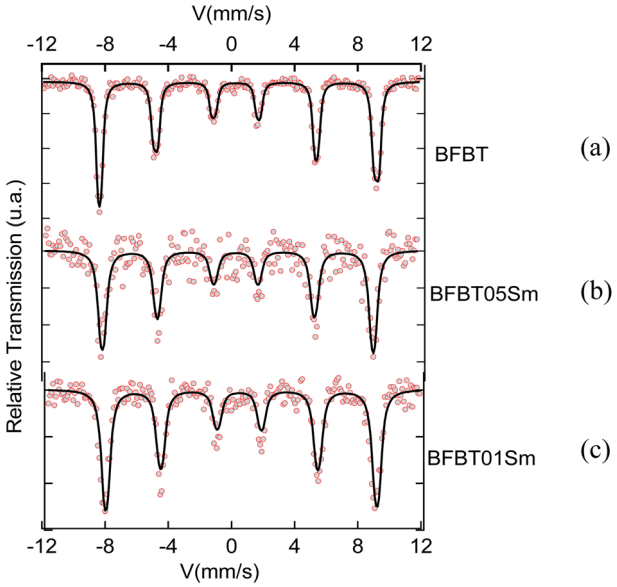

Fig. 6 Mössbauer spectra for BFO (a), BFBT05Sm (b) and BFBT01Sm (c) ceramics.

Table 3 Values of the hyperfine parameters obtained by fitting the experimental spectra recorded at RT

	IS (mm s^{-1})	$\Gamma/2$ (mm s^{-1})	S. Q. (mm s^{-1})	Bhf (kOe)	ω_M	%
BFBT	0.509	0.15	0.51	544	0.991	100
BFBT01Sm	0.549	0.23	0.51	530	0.997	100
BFBT05Sm	0.501	0.22	0.49	529	1.000	100

Data availability

The data that support the findings of this study are available from the corresponding author upon reasonable request.

Conflicts of interest

We confirm that there are no conflicts of interest to declare for this manuscript.

References

1 X. Shan, C. Zhou, Z. Cen, H. Yang, Q. Zhou and W. Li, Bi($Zn_{1/2}$ $Ti_{1/2}$)O_3 modified $BiFeO_3$ –$BaTiO_3$ lead-free piezoelectric ceramics with high temperature stability, *Ceram. Int.*, 2013, **39**(6), 6707–6712.

2 W. Eerenstein, N. D. Mathur and J. F. Scott, Multiferroic and magnetoelectric materials, *Nature*, 2006, **442**(7104), 759–765.

3 M. Kumar, M. Kumar, V. R. Palkar, S. Kuchipudi and S. Suryanarayana, Ferroelectricity in Pure $BiFeO_3$ Ceramic, *Appl. Phys. Lett.*, 2000, **76**, 2764–2766.

4 Y. P. Wang, L. Zhou, M. F. Zhang, X. Y. Chen, J. M. Liu and Z. G. Liu, Room-temperature saturated ferroelectric polarization in BiFeO3 ceramics synthesized by rapid liquid phase sintering, *Appl. Phys. Lett.*, 2004, **84**(10), 1731–1733.

5 D. Radziuk and H. Möhwald, Ultrasonically treated liquid interfaces for progress in cleaning and separation processes, *Phys. Chem. Chem. Phys.*, 2016, **18**(1), 21–46.

6 H. Zhao, Y. Lai, L. Feng, J. Shen, X. Jia, W. Mi, *et al.*, Ferroelectric, ferromagnetic and magneto-capacitance properties of Sm-doped $BiFeO_3$–$BaTiO_3$ solid solution, *Appl. Phys. A*, 2023, **129**(1), 77.

7 H. Singh, A. Kumar and K. L. Yadav, Structural, dielectric, magnetic, magnetodielectric and impedance spectroscopic studies of multiferroic $BiFeO_3$–$BaTiO_3$ ceramics, *Mater. Sci. Eng., B*, 2011, **176**(7), 540–547.

8 H. Krir, F. Gadhoumi, N. Abdelmoula, D. Mezzane and H. Khemakhem, Boosting the optical, dielectric, and ferromagnetic properties of $BiFeO_3$–$BaTiO_3$ ceramics by Eu substitution, *Phys. Rev. B*, 2024, **679**, 415782.

9 X. Xu, T. Guoqiang, R. Huijun and X. Ao, Structural, electric and multiferroic properties of Sm-doped $BiFeO_3$ thin films prepared by the sol–gel process, *Ceram. Int.*, 2013, **39**(6), 6223–6228.

10 W. Sun, J. F. Li, Q. Yu and L. Q. Cheng, Phase transition and piezoelectricity of sol–gel-processed Sm-doped $BiFeO_3$ thin films on Pt(111)/Ti/SiO_2/Si substrates, *J. Mater. Chem. C*, 2015, **3**(9), 2115–2122.

11 K. S. Nalwa and A. Garg, Phase evolution, magnetic and electrical properties in Sm-doped bismuth ferrite, *J. Appl. Phys.*, 2008, **103**(4), 044101.

12 F. Orudzhev, N. Alikhanov, S. Ramazanov, D. Sobola, R. Murtazali, E. Ismailov, *et al.*, Morphotropic Phase Boundary Enhanced Photocatalysis in Sm Doped $BiFeO_3$, *Molecules*, 2022, **27**(20), 7029.

13 J. Zhang, W. Xue, X. Y. Chen and Z. L. Hou, Sm doped $BiFeO_3$ nanofibers for improved photovoltaic devices, *Chin. J. Phys.*, 2020, **66**, 301–306.

14 M. Shariq, D. Kaur and V. S. Chandel, in *Investigation of Structural and Magnetic Properties of Pb Free Multiferroic (BiFeO$_3$)1 − x(BaTiO$_3$)$_x$ Solid Solutions*, 2016, Rhodes, Greece, p. 030018.

15 M. M. Kumar, A. Srinivas and S. V. Suryanarayana, Structure property relations in $BiFeO_3$/$BaTiO_3$ solid solutions, *J. Appl. Phys.*, 2000, **87**(2), 855–862.

16 T. Fan, C. Ji, G. Chen, W. Cai, R. Gao, X. Deng, *et al.*, Enhanced the dielectric relaxation characteristics of $BaTiO_3$ ceramic doped by $BiFeO_3$ and synthesized by the microwave sintering method, *Mater. Chem. Phys.*, 2020, **250**, 123034.

17 H. H. Singh and H. B. Sharma, Enhanced Electrical and Magnetic Properties of Samarium (Sm) Doped Multiferroic Bismuth Ferrite (BFO) Ceramics, *Integr. Ferroelectr.*, 2019, **203**(1), 120–132.

18 M. K. Anupama, B. Rudraswamy and N. Dhananjaya, Investigation on impedance response and dielectric relaxation of Ni-Zn ferrites prepared by self-combustion technique, *J. Alloys Compd.*, 2017, **706**, 554–561.

19 Z. Ma, G. Li, B. Sun, H. Liqiang, W. Gao, Q. Sun, *et al.*, Enhanced electric-field-induced strain in 0.7Bi(1 − x) SmxFeO_3–0.3$BaTiO_3$ lead-free ceramics, *J. Mater. Sci.*, 2020, **55**, 1–11.

20 F. Gadhoumi, A. Lahmar, N. Abdelmoula, M. EL Marssi and H. Khemakhem, in *Investigation of Structural and Magnetic Properties of Pb Free Multiferroic (BiFeO$_3$)$_{1-x}$(BaTiO$_3$)$_x$ Solid Solutions*, Rhodes, Greece, 2021, vol. 877, p. 160323.

21 A. Vorobiev, M. Löffler, E. Olsson and S. Gevorgian, Effect of growth conditions on microstructure of $BiFeO_3$–0.33$BaTiO_3$ films and performance of bulk acoustic wave resonators, *J. Appl. Phys.*, 2014, **115**(8), 084105.

22 D. V. Karpinsky, A. Pakalniškis, G. Niaura, D. V. Zhaludkevich, A. L. Zhaludkevich, S. I. Latushka, *et al.*, Evolution of the crystal structure and magnetic properties of Sm-doped $BiFeO_3$ ceramics across the phase boundary region, *Ceram. Int.*, 2021, **47**(4), 5399–5406.

23 R. A. Malik, A. Hussain, A. Maqbool, A. Zaman, T. K. Song, W. J. Kim, *et al.*, Giant strain, thermally-stable high energy storage properties and structural evolution of Bi-based lead-free piezoceramics, *J. Alloys Compd.*, 2016, **682**, 302–310.

24 J. Anthoniappen, C. S. Tu, P. Y. Chen, C. S. Chen, Y. U. Idzerda and S. J. Chiu, Raman spectra and structural stability in B-site manganese doped $(Bi_{0.5}Na_{0.5})_{0.925}Ba_{0.075}TiO_3$ relaxor ferroelectric ceramics, *J. Eur. Ceram. Soc.*, 2015, **35**(13), 3495–3506.

25 G. Y. Mendez, A. Peláiz Barranco, A. Curcio, A. Rodrigues and J. de los Santos Guerra, Raman spectroscopy study of the La-modified $(Bi_{0.5}Na_{0.5})_{0.92}Ba_{0.08}TiO_3$ lead-free ceramic system, *J. Raman Spectrosc.*, 2019, **17**, 50.

26 J. Bielecki, P. Svedlindh, D. T. Tibebu, S. Cai, S. G. Eriksson, L. Börjesson, *et al.*, Structural and magnetic properties of isovalently substituted multiferroic $BiFeO_3$: Insights from Raman spectroscopy, *Phys. Rev. B*, 2012, **86**(18), 184422.

27 X. Zhang, Y. Sui, X. Wang, Y. Wang and Z. Wang, Effect of Eu substitution on the crystal structure and multiferroic properties of BiFeO3, *J. Alloys Compd.*, 2010, **507**(1), 157–161.

28 R. A. Malik and H. Alrobei, Processing and Characterization of BCZT-Modified $BiFeO_3$–$BaTiO_3$ Piezoelectric Ceramics, *Crystals*, 2021, **11**(9), 1077.

29 M. Kumar, S. Shankar, O. P. Thakur and A. K. Ghosh, Studies on magnetoelectric coupling and magnetic properties of (1 −

x)$BiFeO_3$–*x*$BaTiO_3$ solid solutions, *J. Mater. Sci.:Mater. Electron.*, 2015, **26**(3), 1427–1434.

30 Z. Y. Cheng, R. S. Katiyar, X. Yao and A. S. Bhalla, Temperature dependence of the dielectric constant of relaxor ferroelectrics, *Phys. Rev. B*, 1998, **57**(14), 8166–8177.

31 S. N. Das, A. Pattanaik, S. Kadambini, S. Pradhan, S. Bhuyan and R. N. P. Choudhary, Dielectric and impedance spectroscopy of Ni doped $BiFeO_3$–$BaTiO_3$ electronic system, *J. Mater. Sci.:Mater. Electron.*, 2016, **27**(10), 10099–10105.

32 L. T. Xie, X. X. Zhou, Y. C. Tang, Y. Yin, Y. Hao, J. Pei, *et al.*, Relaxation behavior of BF–BT based ceramics and improved energy storage performance under low electric field, *J. Mater. Sci.:Mater. Electron.*, 2024, **35**(7), 483.

33 J. Rodríguez-Carvajal, M. Hennion, F. Moussa, A. H. Moudden, L. Pinsard and A. Revcolevschi, Neutron-diffraction study of the Jahn–Teller transition in stoichiometric, *Phys. Rev. B*, 1998, **57**(6), R3189–R3192.

34 G. Liu, F. Yang, M. Liu, J. Li, G. Zhang, Z. Jiang, *et al.*, Mossbauer studies of $BiFeO_3$ Mulitiferroic nanoparticles doped with Eu, *Hyperfine Interact.*, 2020, **241**(1), 50.

35 A. Ouertani, Z. Abdelkafi, H. Khemakhem and N. Randrianantoandro, Investigating the influence of Cu and Ti substitution on the structural, optical, and dielectric properties of $BiFeO_3$, *RSC Adv.*, 2024, **14**(20), 14080–14090.

36 A. Tamilselvan, S. Balakumar, M. Sakar, C. Nayek, P. Murugavel and K. Saravana Kumar, Role of oxygen vacancy and Fe–O–Fe bond angle in compositional, magnetic, and dielectric relaxation on Eu-substituted $BiFeO_3$ nanoparticles, *Dalton Trans.*, 2014, **43**(15), 5731–5738.

37 T. R. Paudel, S. S. Jaswal and E. Y. Tsymbal, Intrinsic defects in multiferroic $BiFeO_3$ and their effect on magnetism, *Phys. Rev. B*, 2012, **85**(10), 104409.

38 S. R. Burns, O. Paull, J. Juraszek, V. Nagarajan and D. Sando, The Experimentalist's Guide to the Cycloid, or Noncollinear Antiferromagnetism in Epitaxial $BiFeO_3$, *Adv. Mater.*, 2020, **32**(45), 2003711.

39 A. Agbelele, D. Sando, C. Toulouse, C. Paillard, R. D. Johnson, R. Rüffer, *et al.*, Strain and Magnetic Field Induced Spin-Structure Transitions in Multiferroic $BiFeO_3$, *Adv. Mater.*, 2017, **29**(9), 1602327.

40 H. Fki, M. Koubaa, L. Sicard, W. Cheikhrouhou-Koubaa, A. Cheikhrouhou and S. Ammar-Merah, Influence of Y doping on structural, vibrational, optical and magnetic properties of $BiFeO_3$ ceramics prepared by Mechanical Activation, *Ceram. Int.*, 2017, **43**(5), 4139–4150.

41 S. S. Kumar, N. S. Gajbhiye and A. Banerjee, Structural transformation and enhancement in magnetic properties of single-phase $Bi_{1-x}Pr_xFeO_3$ nanoparticles, *J. Appl. Phys.*, 2013, **113**(20), 203917.